CHAPTER 5

5.1 Introduction

Extensive industrial applications of heavy metals and their indiscriminate indecent disposal into water followed by ensuing its accumulation into water resources leads to continuous deterioration of water quality as well as pose serious health hazards to humans and animals [Gómez et al., 2014]. These metallic species exert detrimental effects due to their non-biodegradable nature as well as their build-up in food chain [Maksin et al., 2012]. Among such toxic metals, Chromium (Cr) has found wide-spread applications in various industries including leather tanning, electroplating, mining, paint and pigment formulation, textile, dyes, wood preservation, cement, metal finishing, stainless steel, alloys, photographic materials etc [Othman et al., 2012; Anirudhan et al., 2013]. Chromium exists commonly in two oxidation states, as either Cr(VI) or Cr(III) ions, among which Cr(VI) has higher mobility in comparison to Cr(III) and is thus contemplated as toxic species [Owlad et al., 2010]. Cr(VI) ions on human contacts are depicted to cause several health complications such as skin irritation, nausea, vomiting, hepatic disease, bronchitis, severe diarrhoea, epigastric pain, pulmonary congestion, ulceration, haemorrhage, including bronchogenic and gastrointestinal carcinoma, etc. [Gueye et al., 2014; Sun et al., 2013; Burks et al., 2014; Brauer and Wetterhahn 1991; Srivastava et al., 2013]. According to The United States Environmental Protection Agency (USEPA) water standards, the maximum limit of chromium in drinking water is 0.1 mg/L which is based on the total chromium [EPA 1990]. However, Cr (VI)

concentration in wastewaters is reported to be 50-100 mg/L [Zhao et al., 2010] which is approximately 1000 times higher than the standards. Therefore, it has become imperative to lower the chromium concentration to the permissible limits by adopting appropriate technologies before its disposal into the environment.

Many low-cost adsorbents such as saw dust, activated carbon, pine needles, cactus leaves, hazelnut shells, sea-weed, fertilizer waste, dead fungal biomass, fly ash, etc. have been investigated for metal removal but most of these exhibit slower adsorption kinetics as well as possess low adsorption capacities [Khosravi et al., 2014; Kuai et al., 2013]. Therefore, it is desirable to develop adsorbents of low cost as well as with higher sorption capacity and faster kinetics. In this respect, interest has been developed towards the application of nanomaterials as metal adsorbents for removal and detoxification of toxic metals due to their large surface which enable them to adsorb larger amounts of metal ions with enhanced adsorption capacity and rapid sorption rate. Additionally, some adsorbents exhibit magnetic properties which allow their complete separation from aqueous phase on application of magnetic field. The regeneration and reuse potential of nano-adsorbents make the adsorption process efficient and economical.

Previous researches have shown that a number of nanoparticles such as alumina, iron-oxide, zirconia, jacobsite, maghemite, nickel oxide, copper oxide and carbon nanotubes have been reported as efficient sorbents for Cr(VI) removal from aqueous solution [Li et al., 2013; Khosravi et al., 2014; Gusain et al., 2014; Sharma et al., 2009; Shyam et al., 2013; Gupta et al., 2011; Sharma et al., 2010; Wu et al., 2012; Albadrin et al., 2012; Srivastava et al., 2014].

The present study explored the adsorption capacity of alumina nanoparticles modified with cetyl trimethyl ammonium bromide (CTAB) for removal of Cr (VI) ions from aqueous solutions along with the effect of various process parameters like initial metal ion concentration, adsorbent dose and pH of the solution on the removal process using Box-Behnken model of experimental design in Response Surface Methodology (RSM).

5.2. Results and discussions

5.2.1 Characterization of nano-alumina after adsorption of chromium

The structural and morphological characterization of nano-alumina before adsorption has been discussed elsewhere (Section 4.2.3, Chapter 4). On comparing the X-ray diffraction pattern of nano-alumina before and after adsorption of chromium, no additional peak appeared demonstrating structural changes did not occur during the process (Figure 5.1).

Similarly, no extra peak appeared in FTIR of nano-alumina after adsorption suggested that the process of removal was physical in nature (Figure 5.2).

Elemental composition of the synthesized nano-alumina was also explored after adsorption through EDS and the spectrum revealed peaks of Cr along with the peaks of Al and O that confirmed its adsorption on the surface (Figure 5.3).

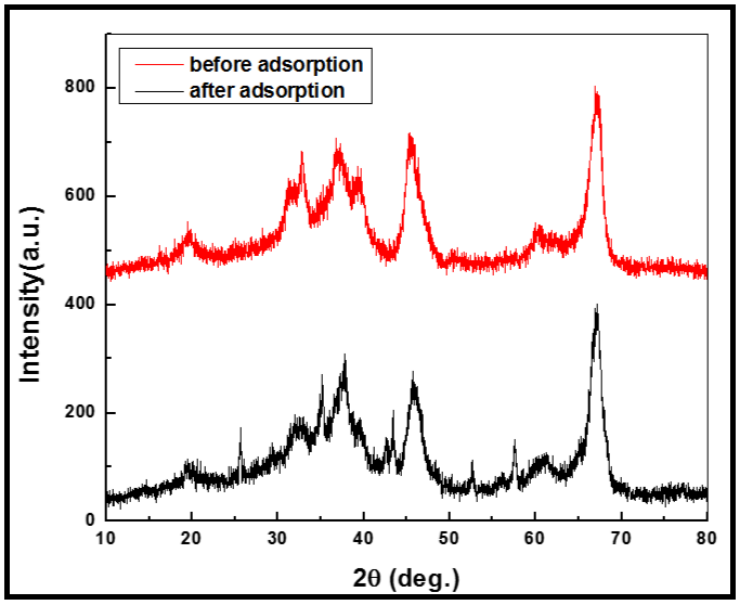

Figure 5.1 XRD pattern of nano-alumina before and after adsorption of Cr(VI) ions

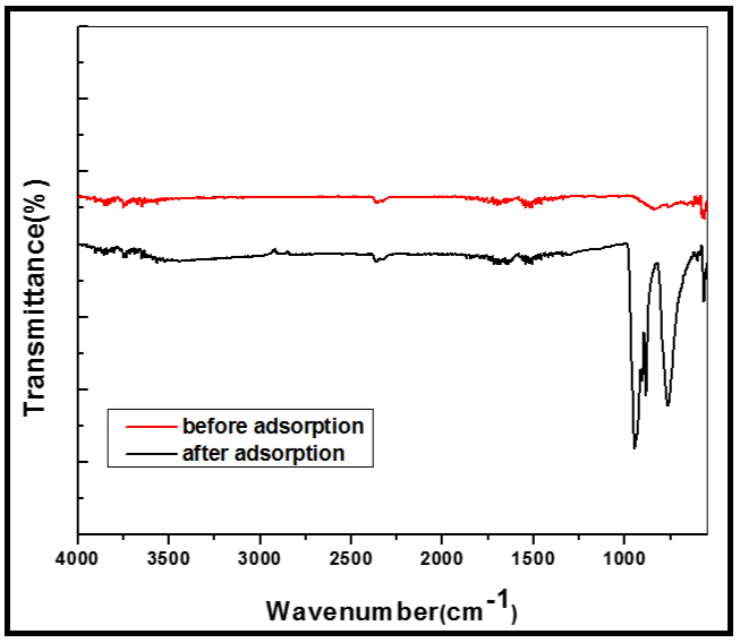

Figure 5.2 FT-IR spectra of nano-alumina before and after adsorption of Cr(VI) ions

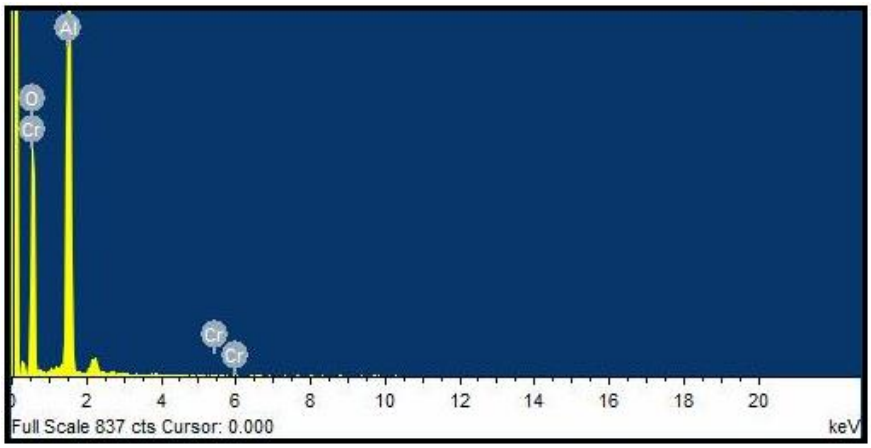

Figure 5.3. EDS pattern of nano-alumina after adsorption of Cr(VI) ions

5.2.2 Adsorption Experiments

The adsorption experiments were conducted in a batch mode and the detailed description has been given in Section 3.7.1 of Chapter 3.

5.2.2.1 Effect of experimental parameters on the removal of chromium from aqueous solution

The results of preliminary experiments conducted for investigation of influence of pH on the process exhibited that acidic conditions favoured the adsorption while increasing pH showed decrease of removal. The percentage of Cr(VI) adsorbed by alumina nanoparticles was minified when the pH of the solution was augmented from 2.0 to 10 (Figure 5.4). The optimal removal of the present system was achieved at pH 2.0, and hence this pH was selected for the rest of the experiments. Similarly, the effect of contact time and was investigated by conducting experiment with 5 mg/L of chromium

solution at different intervals and it was observed from the Figure 5.5 that the adsorption rate for metal ion increases in the beginning and after 60 min the adsorption rate become roughly steady and finally adsorption equilibrium was achieved within 60 min after which no significant change was marked in the removal of metal ions. Likewise, removal percent of chromium upgraded with increased dosage of adsorbent keeping other experimental conditions incessant (Figure 5.6). At lower concentration, the ratio between free sites on the adsorbent surface and metal ions is very high in comparison to higher concentration and hence the removal percentage is higher for lower concentration and vice versa as depicted in Figure 5.7. It was found that removal decreased from on escalating concentration from 5 mg/L to 25 mg/L.

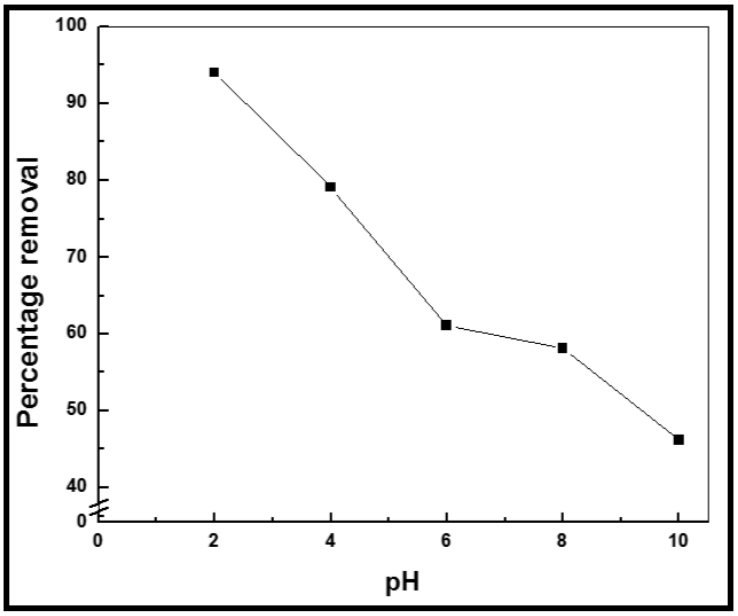

Figure 5.4 Effect of initial pH on removal (%) of chromium from aqueous solution on nano-alumina (Initial concentration= 10 mg/L, adsorbent dose= 10g/L, Temperature= 303K)

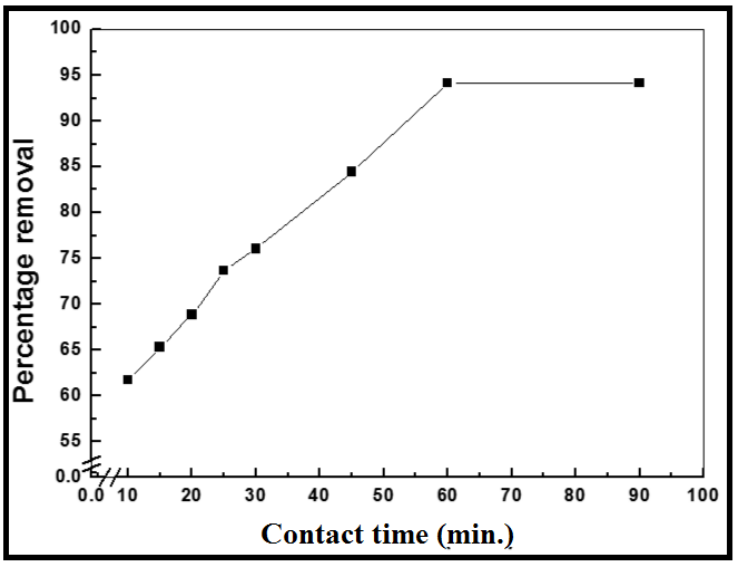

Figure 5.5 Effect of contact time on removal (%) of chromium from aqueous solution on nano-alumina (Initial concentration=10mg/L, Initial pH=2.0, Initial dose=10g/L, Temperature= 303K)

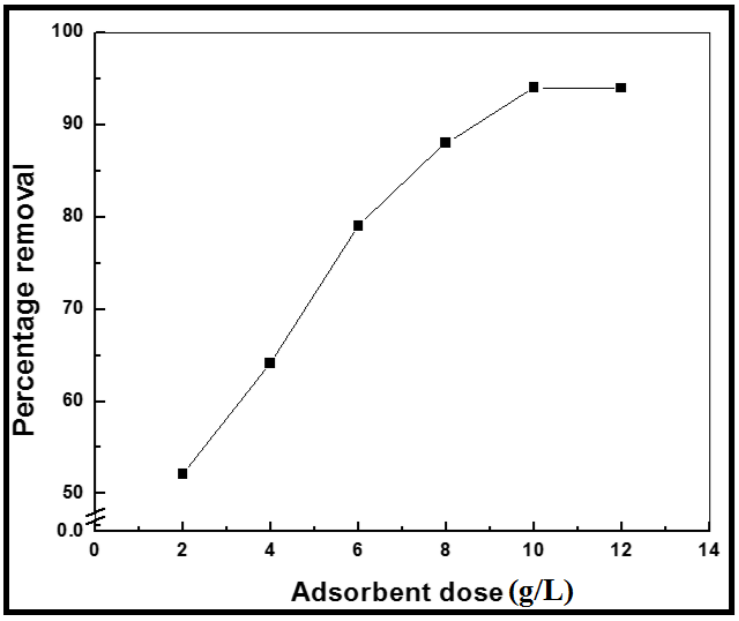

Figure 5.6 Effect of adsorbent dose on removal (%) of chromium from aqueous solution on nano-alumina (Initial pH=2.0, Initial concentration =10mg/L, Temperature=303K)

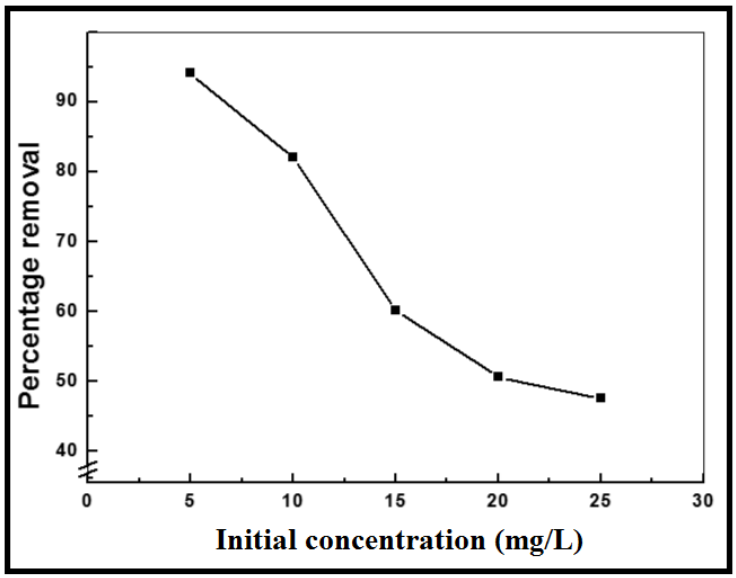

Figure 5.7 Effect of initial concentration on removal (%) of chromium from aqueous solution on nano-alumina (Initial pH= 2.0, Initial dose= 10g/L, Temperature=303 K)

5.2.2.2 Design of experiment and data analysis for adsorption of chromium (VI) on nano-alumina

The adsorption experiments based on the design matrix of Box-Behnken design of RSM (Section 3.7.2.2, Chapter 3) were conducted for obtaining the response corresponding to the independent variables addressed in the experimental design matrix by applying quadratic model and corresponding results obtained has been presented in Table 5.1.

Table 5.1 Box-Behnken designed experimental runs for removal of chromium on nano-alumina

Run Order	Concentration (mg/L)	pH	Dose (g/L)	Percent removal
1	5	2	11	94.02
2	25	2	11	78.46
3	5	10	11	82.05
4	25	10	11	21.03
5	5	6	2	70.09
6	25	6	2	49.75
7	5	6	20	88.03
8	25	6	20	71.28
9	15	2	2	24.22
10	15	10	2	16.24
11	15	2	20	54.13
12	15	10	20	26.21
13	15	6	11	38.18
14	15	6	11	36.18
15	15	6	11	38.18

On the basis of experimental findings, the empirical relationship between the response and the independent variables namely initial concentration, pH and adsorbent dose in the coded units is presented in the form of following polynomial regression equation for removal (%) of chromium designated by Y:

$$Y = 92.2932 - 10.4946\,(\text{concentration}) - 5.9203\,(\text{pH}) + 64.1889\,(\text{adsorbent dose}) + 0.3548\,(\text{concentration})^2 - 0.2565\,(\text{pH})^2 - 20.046\,(\text{adsorbent dose})^2 - 0.2842\,(\text{concentration} \times \text{pH}) + 0.2243\,(\text{concentration} \times \text{adsorbent dose}) - 3.116\,(\text{pH} \times \text{adsorbent dose}) \quad (5.1)$$

In order to support the hierarchical nature of this model, insignificant terms were still maintained in this study and have been included in the given regression equation [Dahlan et al., 2008]. In the quadratic equation (Eq. 5.1), the magnitude of coefficient portrays the intensity while the sign before the coefficient indicates nature of influence (positive or negative) of the particular variable on the response. A positive sign of a factor means that the response is improved when the factor level augments and a negative effect of the factor revealed that the response is suppressed with the increase in factor level [Sarkar et al., 2011]. Upon regression analysis, the regression equation for removal of chromium with alumina nanoparticles yielded regression coefficient $R^2 = 96.51$, higher than the R^2 (adj.) = 90.23 (Table 5.2) that validates the process of adsorption in the given range of experimental conditions. The parameters bearing positive sign before their corresponding coefficients inclined to increase the chromium removal (%) and vice versa [Sarkar et al., 2011].

From the equation, it has been deciphered that adsorbent dose is the most dominating parameter having positive sign before its coefficient followed by pH and concentration. Negative sign before coefficients of both pH and concentration suggested the decrease in chromium removal (%) with increase in pH and concentration.

Table 5.2 Estimated regression coefficients for removal of chromium on nano-alumina

Term	Coef	SE Coef	T	P
Constant	92.2932	22.4671	4.108	0.009
Conc	-10.4946	1.5785	-6.648	0.001
pH	-5.9203	3.9463	-1.5	0.194
Dose	6.499	39.4632	1.627	0.165
Conc*Conc	0.3548	0.0428	8.294	0
pH* pH	-0.2565	0.2674	-0.96	0.381
Dose*Dose	-0.2005	26.7373	-0.75	0.487
Conc*pH	-0.2842	0.1028	-2.766	0.04
Conc*Dose	0.2243	1.0275	0.218	0.836
pH*Dose	-0.312	2.5688	-1.213	0.279
S =8.22027	**PRESS =5369.37**			
R-Sq =96.51%	**R-Sq(pred) =44.52%**		**R-Sq(adj) =90.23%**	

5.2.2.3 Analysis of variance (ANOVA)

In order to ensure a good model, statistical testing was performed by applying analysis of variance (ANOVA) (Section 3.7.2.3, Chapter 3) and the results were presented in Table 5.3.

Table 5.3 Analysis of variance for removal of chromium on nano-alumina

Source	DF	Seq SS	Adj SS	Adj MS	F	P
Regression	9	9340.32	9340.32	1037.81	15.36	0.004
Linear	3	3788.44	4012.55	1337.52	19.79	0.003
Concentration	1	1615.12	2986.74	2986.74	44.2	0.001
pH	1	1385.87	152.08	152.08	2.25	0.194
Dose	1	787.45	178.78	178.78	2.65	0.165
Square	3	4932.4	4932.4	1644.13	24.33	0.002
Concentartion*Concentration	1	4839.14	4648.1	4648.1	68.79	0
pH*pH	1	55.29	62.21	62.21	0.92	0.381
Dose*Dose	1	37.98	37.98	37.98	0.56	0.487
Interaction	3	619.48	619.48	206.49	3.06	0.13
Concentration*pH	1	516.84	516.84	516.84	7.65	0.04
Concentration*Dose	1	3.22	3.22	3.22	0.05	0.836
pH*Dose	1	99.42	99.42	99.42	1.47	0.279
Residual error	5	337.86	337.86	67.57		
Lack-of-Fit	3	335.21	335.21	111.74	84.29	0.012
Pure	2	2.65	2.65	1.33		
Total	14	9678.19				

In present case, ANOVA study exhibited that the regression model is significant as large F-value and a low P value [Esfandiar et al., 2014]. Among linear effect, concentration is the dominant parameter among other having sum of squares (Seq SS) value of 1615.12 followed by pH and adsorbent dose. Similarly, among square effect conc*conc was dominant and among interactive effect conc*pH was found significant on the basis of sum of squares value.

5.2.2.4 Interaction effect of initial Cr(VI) concentration and adsorbent dose

The adsorption experiments based on the matrix predicted by the selected model were conducted with the predetermined concentration range and the desired adsorbent dosage to evaluate their combined effect on the percent removal of hexavalent chromium ions from the aqueous solutions. From the regression equation it is evident that concentration is a major parameter in the adsorption process with coefficient having negative sign that indicates decrease in percent removal with increase in the concentration of solution. This behavior can be attributed to the saturation of active sites available on the adsorbent surface with increase in the concentration of solution and vice a versa. The graphical explication of the interactions of the result of experimentation was presented in the form of contour and surface plots as shown in Figures 5.8a and 5.8b. The interactive effect of concentration and adsorbent dose depicted that maximum removal was achieved at low metal concentration and higher adsorbent dose due to greater availability of active sites for metal ions present in aqueous solutions (Runs “1 and 9”) and (Runs “6 and 7”). Conversely, at lower adsorbent dose and higher metal ion concentration a significant decrease in the removal is observed.

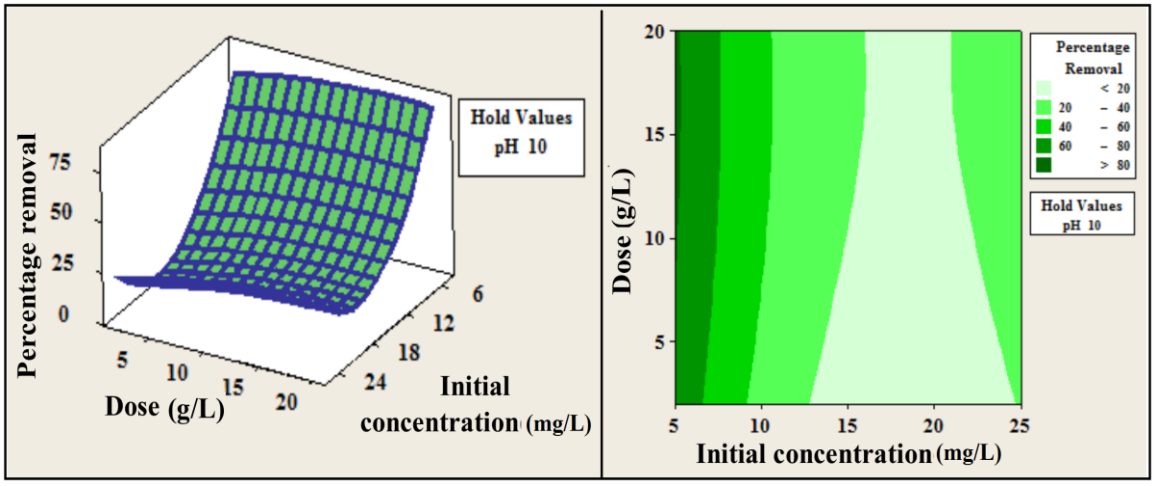

Figure 5.8. (a) Surface plot; and (b) Contour plot of percentage removal vs. dose and concentration at hold value of pH at 10

5.2.2.5 Interaction effect of pH and adsorbent dose

pH is acknowledged as the most important parameter playing a significant role in the metal removal processes. It is reported that variation in pH of solution greatly affects the surface of the adsorbent and degree of ionization in solution. In solution, chromium exists as negatively charged ions such as $HCrO_4^{2-}$, CrO_4^{2-}, $Cr_2O_7^{2-}$ and $Cr_4O_{13}^{2-}$ and their existence is entirely dependent upon the pH of the solution. At lower pH, $HCrO_4^{2-}$ is the dominant species and with a decrease in pH, the adsorbent surface tends to become more positively charged resulting into increased electrostatic interaction between negative Cr species and positive surface of adsorbent [Sharma et al., 2010]. This increased interaction lead to the increased removal of adsorbate ions from solutions with lowering of pH. In the regression equation pH also bears a negative charge on its coefficient which indicates a remarkable decrease in the removal of adsorbate on increase in pH of the solution

[Bajpai et al., 2012]. Similarly, the adsorbent dose with positively charged coefficient suggests that on an increment in the dose of adsorbent the percent removal also increases. Increase in amount of adsorbent results into introduction of a number of unsaturated surface active sites. The interactive effect of both these variables upon adsorption is shown in Figure 5.9a and 5.9b. It has been observed that optimum removal is achieved at low pH (i.e. acidic condition) and high dose (Runs "1 and 8") and (Runs "10 and 11"). Conjointly, increased number of positive species and surface active sites are held responsible for increased percent removal of adsorbate ions.

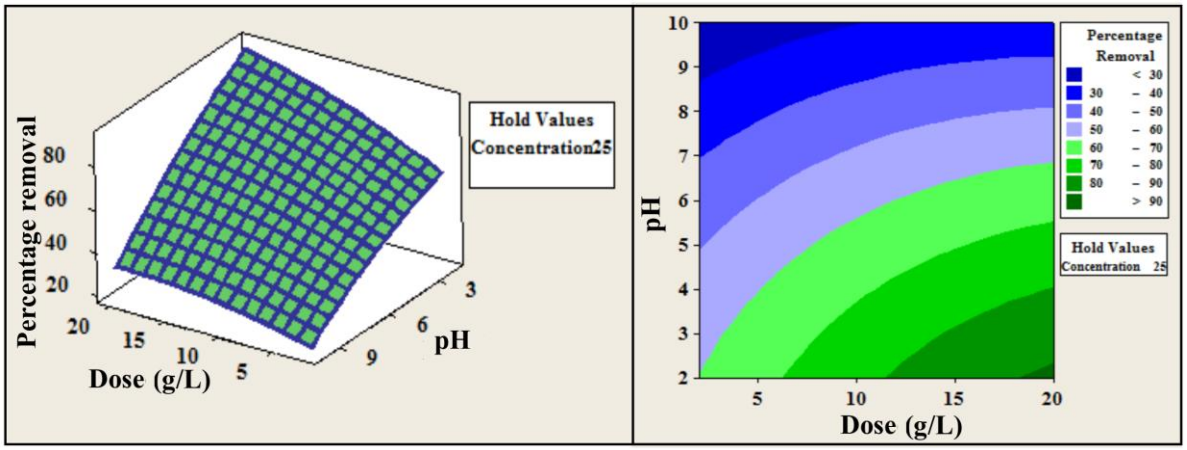

Figure 5.9 (a) Surface plot; and (b) Contour plot of percentage removal vs. pH and dose at hold value of concentration at 25 mg/L

5.2.2.6 Interaction effect of pH and initial Cr(VI) concentration

The combined effect of pH and initial metal ion concentration on the removal process has been studied and the results are depicted in the form of surface and contour

plots as shown in Figure 5.10a and 5.10b. It has been estimated that increasing initial concentration and pH, keeping dose constant, removal percent decreases significantly (Runs "1 and 4") and (Runs "8 and 11"). This might be due to the greater ratio of available surface for adsorbate ions at low concentration whereas at higher concentration this ratio decreases thereby decreasing the overall removal of adsorbate ions.

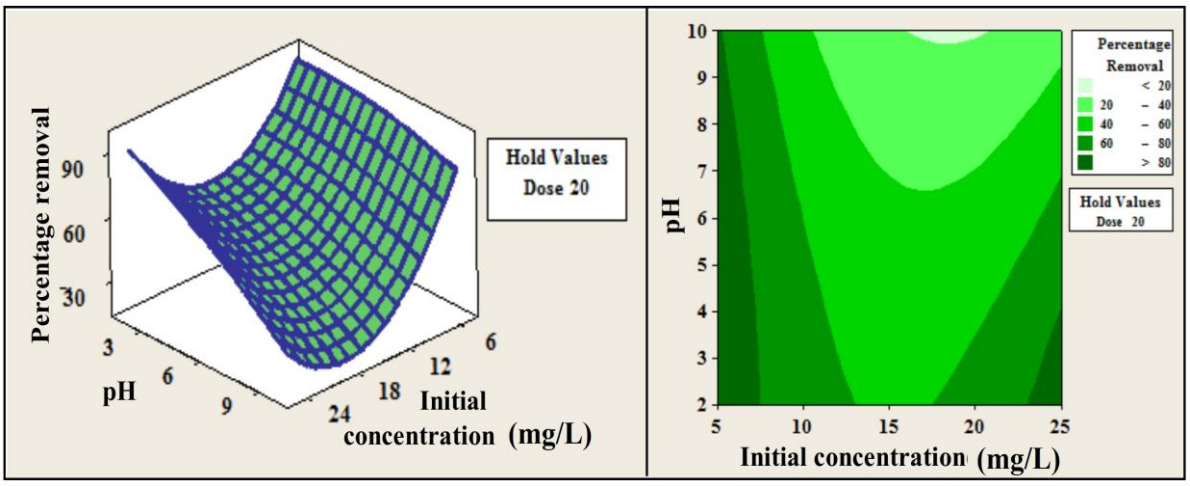

Figure 5.10 (a) Surface plot; and (b) Contour plot of percentage removal vs. pH and concentration at hold value of dose at 20 g/L

5.2.2.7 Interpretation of process optimization of removal (%) of chromium on nano-alumina

The optimum value for desired response was predicted by response optimization plot as shown in Figure 5.11. It predicted the optimum value for 94% removal of Cr(VI) from aqueous solutions via the process of adsorption on alumina nanoparticles for the given model (pH 2.03, initial concentration 5 mg/L, adsorbent dose 20 g/L) with the desirability score 1.00. In order to verify the efficacy of model, confirmatory experiments

were conducted at the predefined conditions. Further, for the confirmation experiment pH of the solution was rounded off to 2.0 and the experimental results were analyzed.

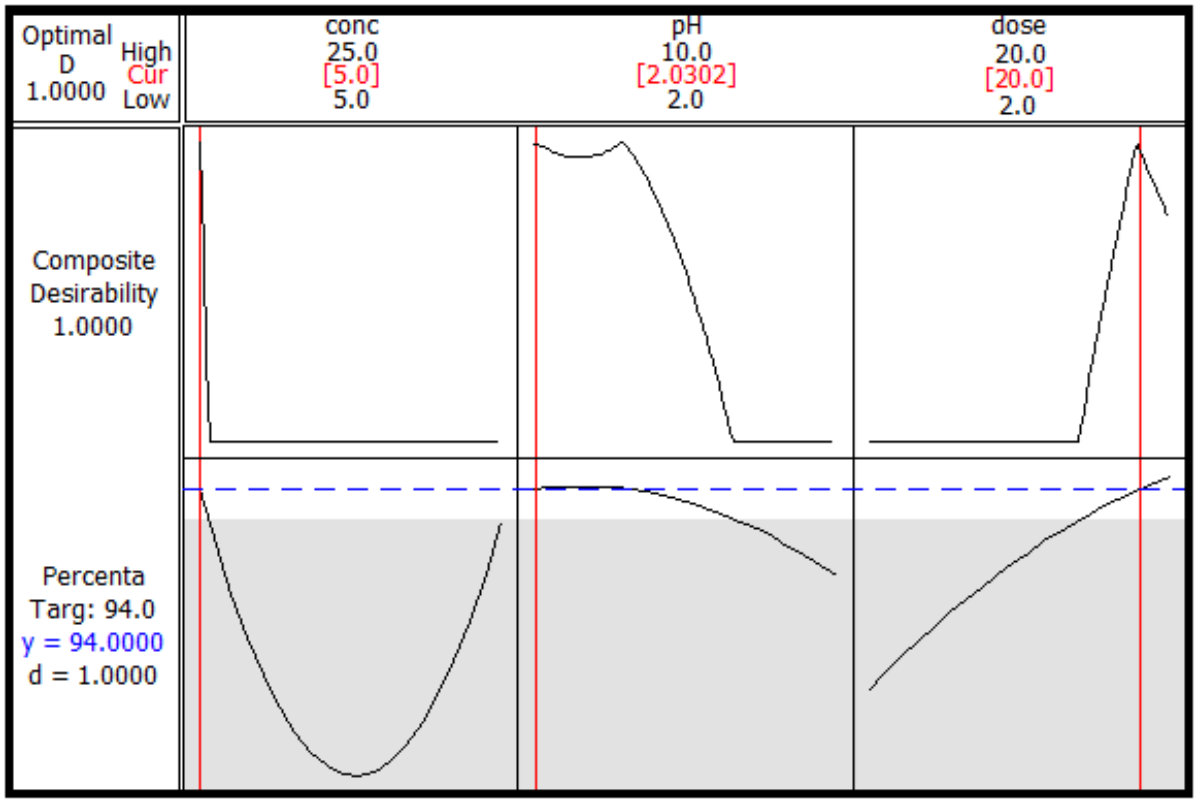

Figure 5.11 Response optimization plot for chromium removal on nano-alumina

However, results showed certain degree of variation than that of predicted by model. The experimental values of the model together with the percentage error difference between the experimental and predicted values have been tabulated in Table 5.4.

Table 5.4 Confirmation experiments for removal of chromium on nano-alumina

S. No.	Concentration (mg/L)	pH	Dose (g/L)	Experimental values (%)	Predicted values (%)
1	5	2	20	94.13	95.69
2	25	2	20	87.35	91.81
3	10	2	20	86.03	90.54

5.2.3 Adsorption isotherm study

The equilibrium adsorption isotherm, in general furnishes useful information regarding properties and tendency of adsorbent toward adsorbate at given condition at equilibrium which is requisite for modelling analysis, operational design and feasibility of the adsorption system [Altin et al., 1998]. In the present study, the equilibrium data incurred for Cr(VI) removal was examined with two parameters isotherm viz. Langmuir and Freundlich to ascertain the most appropriate model explaining the equilibrium data. In order to achieve the best fit isotherm, linear and non-linear analyses of adsorption equilibrium data was performed.

The following linear and non-linear equations of Langmuir and isotherm model were used [Sharma et al., 2008; Langmuir, 1916]:

$$C_e/q_e = 1/bQ^o + C_e/Q^o \quad (5.2)$$

$$q_e = b\ Q^o C_e / 1 + bC_e \quad (5.3)$$

where, C_e (mg/l) is the equilibrium concentration of the solute, q_e (mg/g) is amount adsorbed at equilibrium and Q^0 (mg/g) and b (L/mg) are constants related to the adsorption capacity and energy of adsorption, respectively.

Freundlich isotherm model was fitted through following linear and non-linear equations [Freundlich, 1906; Allen and McKay, 1980]:

$$\log q_e = \log K_F + 1/n \log C_e \quad (5.4)$$

$$q_e = K_F C_e^{1/n} \quad (5.5)$$

where, K_F and n are the Freundlich constants. Here, n giving a sign of how congruous the adsorption process is, and K_F (mg/g(L/mg)$^{1/n}$) represents the quantity of metal ion adsorbed on the adsorbent for a unit equilibrium concentration.

5.2.3.1 Linear analysis of adsorption isotherm

Linear equations of Langmuir and Freundlich adsorption isotherm models were considered to discuss the equilibrium characteristics of the adsorption process in linear approach. The values of theoretical maximum adsorption capacity, Q^0 (mg g^{-1}) and Langmuir adsorption constant b (L mg^{-1}) were obtained from the slope and intercept of the plot of C_e/q_e vs. C_e, respectively (Figure 5.12) and the parameters of Freundlich isotherm model such as the capacity, K_F (mg g^{-1}) and intensity, n (g L^{-1}) of the adsorption were calculated from the intercept and slope of the linear plot of ln q_e vs. ln C_e, respectively as shown in Figure 5.13.

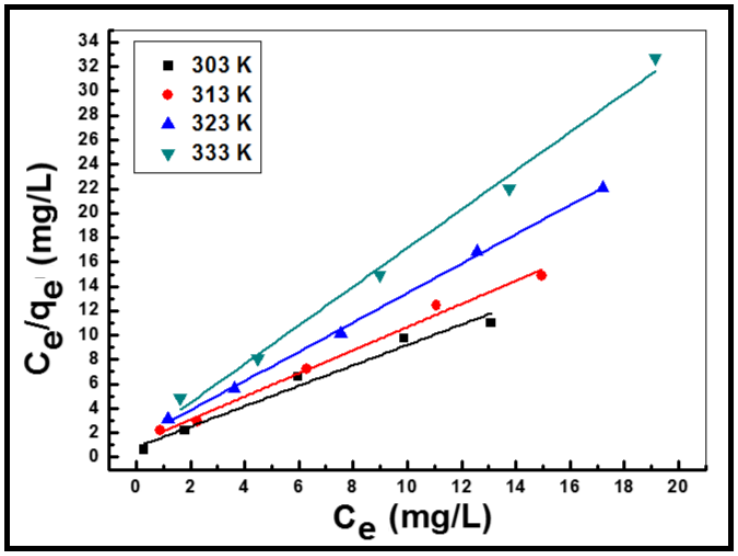

Figure 5.12 Linear Langmuir isotherm plot of Cr(VI) removal on nano-alumina (symbols represent the experimental data and straight lines represent the data estimated by the model)

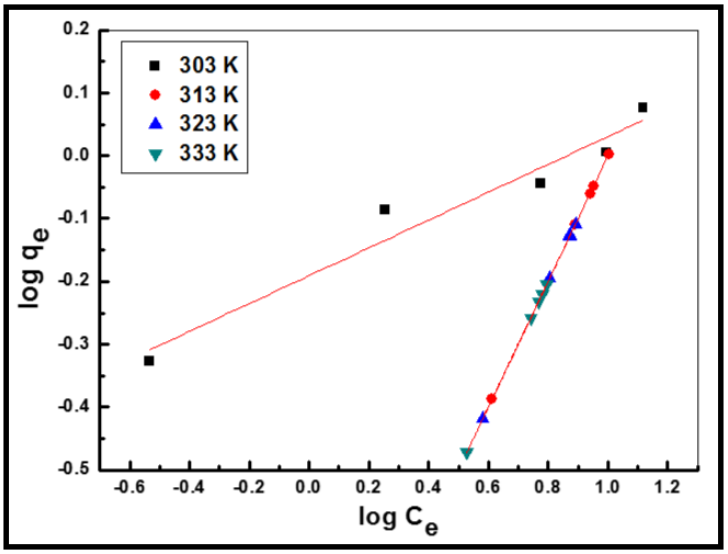

Figure 5.13 Linear Freundlich isotherm plot of Cr(VI) removal on nano-alumina (symbols represent the experimental data and straight lines represent the data estimated by the model)

The fitness of experimental data was evaluated at different temperatures. The high correlation coefficient at all temperatures exhibited that Langmuir model provides the best correlation and thus applicable for interpretation of the experimental data on the whole concentration range (Table 5.5).

Table 5.5 Langmuir and Freundlich isotherm parameters for linear analysis for adsorption of chromium from aqueous solution on nano-alumina

Analysis	**Linear**									
Isotherm	**Langmuir Parameters**					**Freundlich Parameters**				
Temperature (K)		**303**	**313**	**323**	**333**		**303**	**313**	**323**	**333**
Constants	**Q^o (mg/g)**	1.19	1.05	0.83	0.64	**K_F (mg/g $(L/mg)^{1/n}$)**	0.64	0.1	0.1	0.1
	b (L/mg)	1.00	0.80	0.84	1.20	**n**	4.5	1	1	1
Coefficient of determination (R^2)		0.992	0.982	0.969	0.985		0.939	0.671	0.543	0.695

5.2.3.2 Non-linear analysis of adsorption isotherm

Non-linear analysis was performed by altering in-built functions namely Langmuir EXT 1 (Figure 5.14), and Freundlich EXT (Figure 5.15) of origin. In addition to that, user defined isotherm function was used in origin. In user defined equation, initial

parameter was taken as numerically one. On curve fitting, both the in-built functions as well as customised user defined functions (Figure 5.16 and Figure 5.17) depicted significant differences between the experimental data and data predicted by the models at all the pre-defined temperatures (Table 5.6 and 5.7).

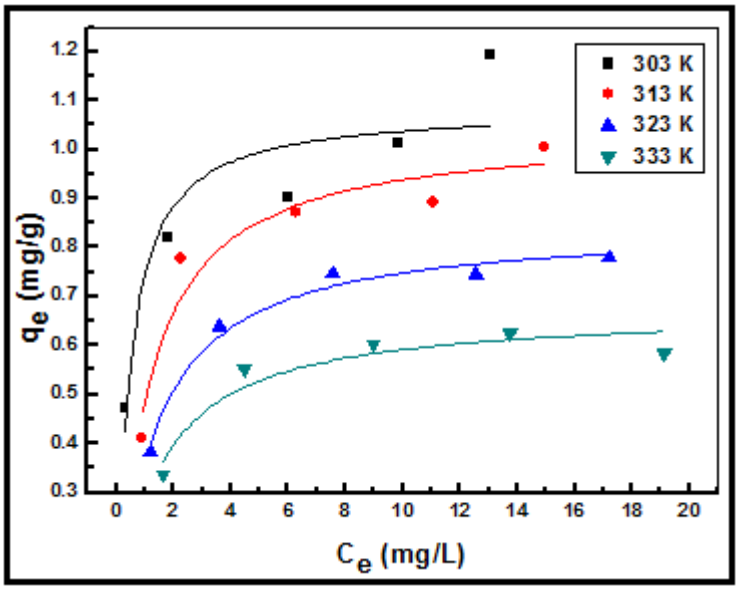

Figure 5.14 Non-linear Langmuir isotherm plot of chromium removal on nano-alumina obtained by in-built Microcal origin function (symbols represent the experimental data and lines represent the data estimated by the model)

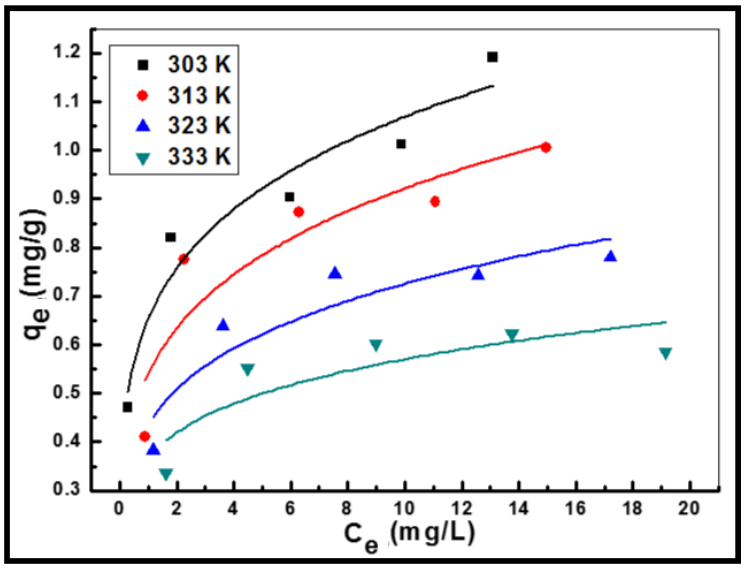

Figure 5.15 Non-linear Freundlich isotherm plot of chromium removal on nano- alumina obtained by in-built Microcal origin function (symbols represent the experimental data and lines represent the data estimated by the model)

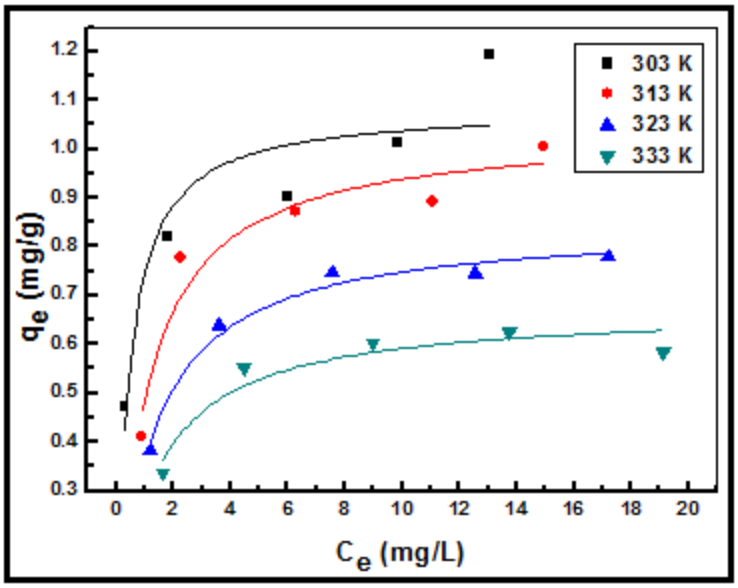

Figure 5.16 Non-linear Langmuir isotherm plot of chromium removal on nano-alumina obtained by customized Microcal origin function (symbols represent the experimental data and lines represent the data estimated by the model)

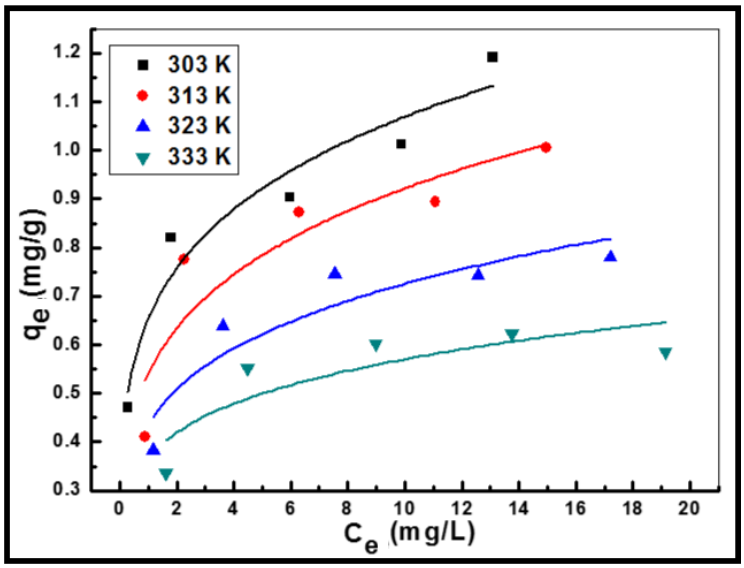

Figure 5.17 Non-linear Freundlich isotherm plot of chromium removal on nano-alumina obtained by customized Microcal origin function (symbols represent the experimental data and lines represent the data estimated by the model)

Table 5.6 Langmuir and Freundlich isotherm parameters for non-linear analysis obtained by in-built Microcal origin functions for adsorption of chromium from aqueous solution on nano-alumina

Analysis	**Non-linear**									
Isotherm	**Langmuir Parameters**					**Freundlich Parameters**				
Temperature (K)		**303**	**313**	**323**	**333**		**303**	**313**	**323**	**333**
Constants	**Q^o (mg/g)**	1.08	1.04	0.85	0.67	**K_F (mg/g (L/mg)$^{1/n}$)**	0.65	0.54	0.43	0.37
	b (L/mg)	2.22	0.89	0.75	0.73	**n**	0.21	0.23	0.22	0.19
Coefficient of determination (R^2)		0.832	0.913	0.977	0.892		0.922	0.785	0.819	0.654

Table 5.7 Langmuir and Freundlich isotherm parameters for non-linear analysis obtained by customized Microcal origin functions for adsorption of chromium from aqueous solution on nano-alumina

Analysis	**Customized**									
Isotherm	**Langmuir Parameters**					**Freundlich Parameters**				
Temperature (K)		**303**	**313**	**323**	**333**		**303**	**313**	**323**	**333**
Constants	**Q^o (mg/g)**	1.08	1.04	0.85	0.67	**K_F (mg/g $(L/mg)^{1/n}$)**	0.65	0.54	0.43	0.37
	b (L/mg)	2.22	0.89	0.75	0.73	**n**	4.67	4.29	4.51	5.24
Coefficient of determination (R^2)		0.963	0.947	0.983	0.986		0.922	0.785	0.819	0.654

On comparing both linear as well as non-linear analyses for isotherm parameter determination, linear analysis was preferred over non-linear approach for isotherm parameter determination on the basis of high R^2 adj. values.

5.2.4 Adsorption kinetic modeling

Adsorption process, in general is supposed to be administered by one or more steps (e.g. film diffusion, intra-particle diffusion, and/or pore diffusion). In order to investigate the rate-controlling step, the mechanism of interaction of adsorbent and adsorbate, rate of uptake of metallic species as contaminant the adsorption data has been fitted to kinetic models, namely pseudo-first-order, pseudo-second-order and intra-particle diffusion

models [Uma et al., 2013]. Linear and non-linear analyses were performed similar to the adsorption isotherm for accomplishing the best fit kinetic model

The pseudo-first-order kinetic model has been widely used to predict the sorption kinetics and can be expressed by the following linear and non-linear equations [Hodaifa et al., 2013]:

$$dq/dt = k_1 (q_e - q_t) \quad (5.6)$$

$$ln (q_e - q_t) = ln\ q_e - k_1 t \quad (5.7)$$

$$q_t = q_e (1 - exp (-k_1 t)) \quad (5.8)$$

where, k_1(min^{-1}) is the first order rate constant, q_e and q_t are the amount of adsorbate species adsorbed on adsorbent at equilibrium and at any time, t, respectively.

Pseudo-second order model is based on the assumption that the rate limiting step is chemi-sorption in nature. The model is represented in the form of following linear and non-linear equations [Ho and McKay, 1998]:

$$dq/dt = k_2 (q_e - q_t)^2 \quad (5.9)$$

$$q_t = k_2 q_e^2\ t / 1 + k_2\ q_e\ t \quad (5.10)$$

where, k_2(g mg^{-1} min^{-1}) is the rate constant for pseudo-second-order model equation.

5.2.4.1 Linear analysis of adsorption kinetics

The kinetic parameters, k_1 and q_e for the pseudo-first-order model (Lagergren model), through linear approach was determined from the slope and intercept of the plot of log (q_e-q_t) vs. t, respectively (Figure 5.18). For the pseudo-second-order kinetic model

the plot of t/q_t vs. t yielded a straight line from which k_2 and the equilibrium adsorption capacity (q_e) were calculated from the intercept and slope, respectively as shown in Figure 5.19. The values of different parameters as determined from the linear analysis of pseudo-first-order and pseudo-second-order kinetic models along with their corresponding correlation coefficients were presented in Table 5.8.

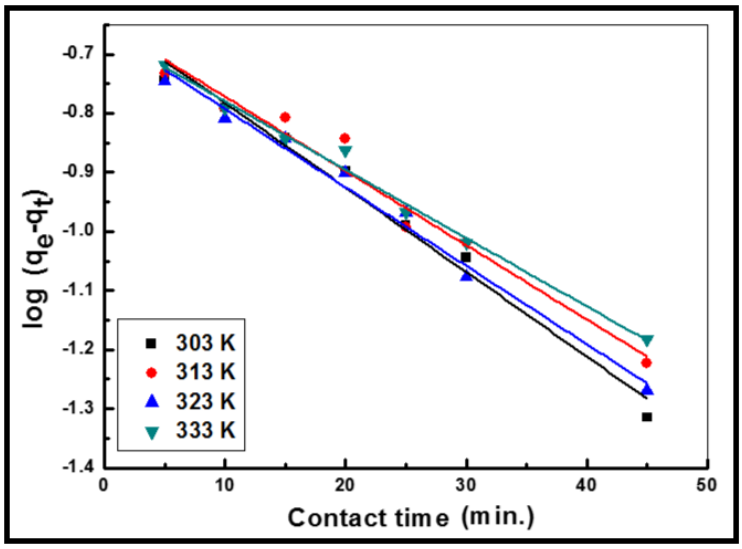

Figure 5.18 Linear pseudo-first order plot of chromium removal on nano-alumina (symbols represent the experimental data and straight lines represent the data estimated by the model)

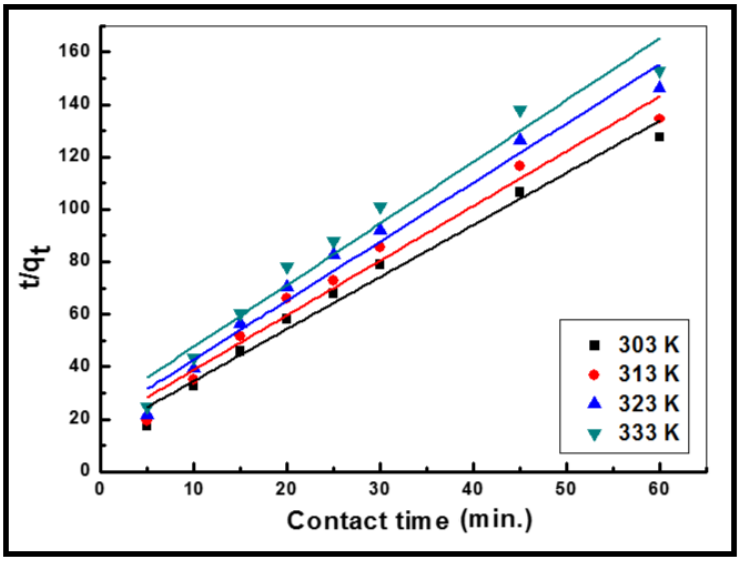

Figure 5.19 Linear pseudo-second order plot of chromium removal on nano-alumina (symbols represent the experimental data and straight lines represent the data estimated by the model)

It was found that q_e(cal) values from pseudo-first-order model were not reasonably close to experimental q_e(exp) values which showed that the system did not followed pseudo-first-order model. In pseudo-second-order kinetic model, the values of q_e(cal) were very close to q_e(exp) with high value of correlation coefficient (R^2). Thus, it was deduced from the value of R^2 and closeness of experimental and theoretical adsorption capacity (q_e) that pseudo-second order kinetic model better explained the experimental data on linear analysis.

Table 5.8 Pseudo-first order and pseudo-second order kinetic parameters for linear analysis and non-linear analysis by Microcal origin for adsorption of chromium from aqueous solution on nano-alumina

Kinetic model	**Pseudo-first order Parameter**						
Analysis		**Linear**			**Non-linear**		
Temperature (K)	**q_e (exp.)**	**q_e (mg/g)**	**k_1 (1/min)**	**R^2 adj.**	**q_e (mg/g)**	**k_1 (1/min)**	**R^2 adj.**
303	0.47	0.23	-0.033	0.980	0.39	0.184	0.351
313	0.44	0.23	-0.029	0.961	0.37	0.159	0.342
323	0.41	0.22	-0.031	0.985	0.34	0.139	0.432
333	0.38	0.22	-0.027	0.988	0.33	0.115	0.512
Kinetic model	**Pseudo-second order Parameter**						
Analysis		**Linear**			**Non-linear**		
Temperature (K)	**q_e (exp.)**	**q_e (mg/g)**	**k_2 ($g.mg^{-1} min^{-1}$)**	**R^2 adj.**	**q_e (mg/g)**	**k_2 ($g.mg^{-1} min^{-1}$)**	**R^2 adj.**
303	0.47	0.50	4.35	0.981	0.44	0.25	0.692
313	0.44	0.48	4.11	0.970	0.42	0.21	0.659
323	0.41	0.44	3.99	0.972	0.39	0.18	0.719
333	0.38	0.42	3.73	0.959	0.38	0.15	0.745

5.2.4.2 Non-linear analysis of adsorption kinetics

In-built functions of Microcal origin namely Langmuir EXT 1 and BoxLucas 1 were altered for curve fitting during non-linear analysis of adsorption data to coincide with pseudo-first order (Figure 5.20) and pseudo-second order (Figure 5.21) kinetic equations respectively. The user defined isotherm function was also used in which initial parameter was taken as numerically one similar to that of the non-linear analysis of isotherm (Figures 5.22 and 5.23).

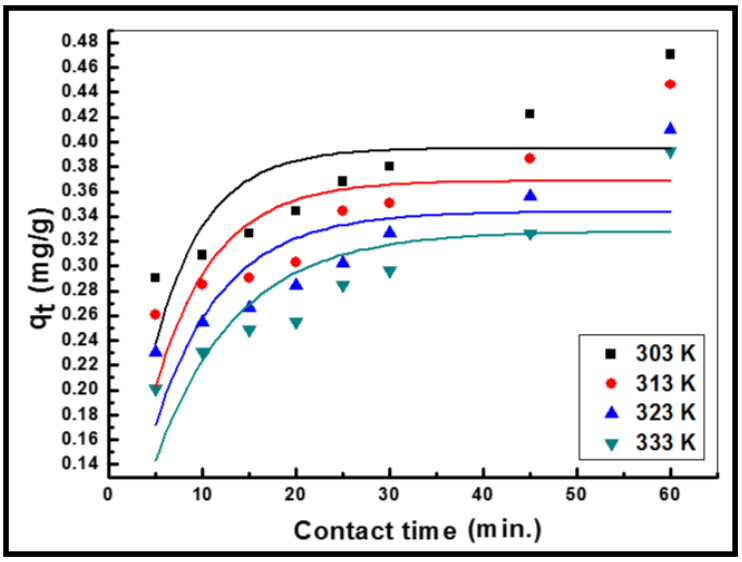

Figure 5.20 Non-linear pseudo-first order plot of chromium removal on nano- alumina obtained by in-built Microcal origin function (symbols represent the experimental data and lines represent the data estimated by the model)

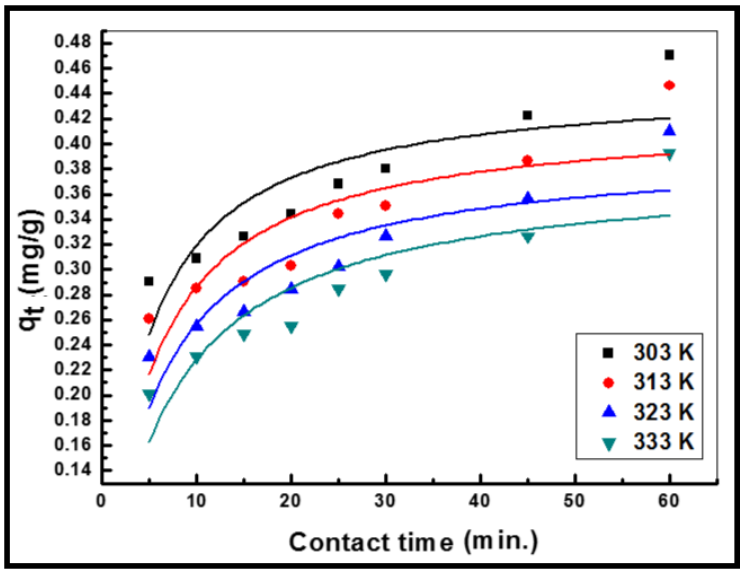

Figure 5.21 Non-linear pseudo-second order plot of chromium removal on nano-alumina obtained by in-built Microcal origin function (symbols represent the experimental data and lines represent the data estimated by the model)

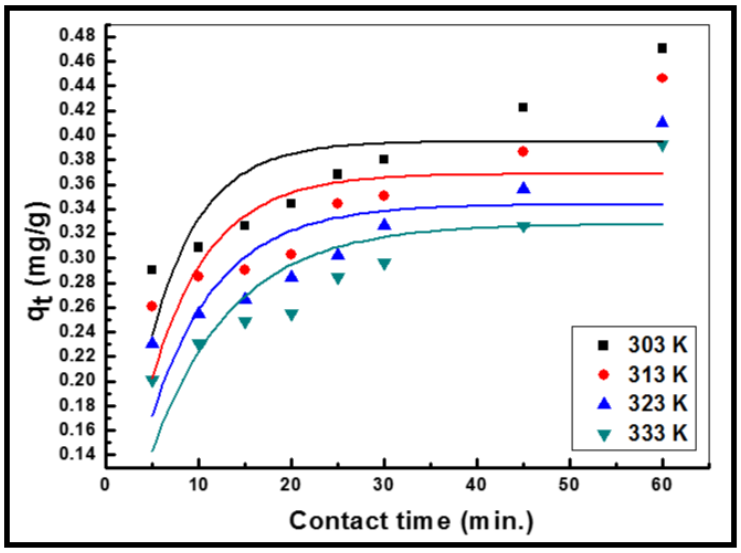

Figure 5.22 Non-linear pseudo-first order plot of chromium removal on nano- alumina obtained by customized Microcal origin function (symbols represent the experimental data and lines represent the data estimated by the model)

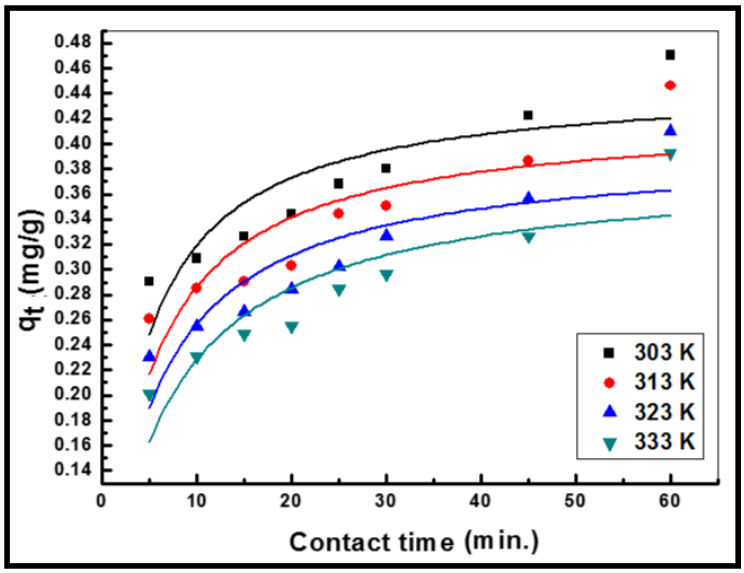

Figure 5.23 Non-linear pseudo-second order plot of chromium removal on nano-alumina obtained by customized Microcal origin function (symbols represent the experimental data and lines represent the data estimated by the model)

Non-linear approach showed a significant difference between the experimental data and data estimated by both the in-built and customized Microcal origin functions (Table 5.8 and 5.9). Thus, on the basis of high R^2 adj. value, linear approach of kinetic analysis was more appropriate for determination of kinetic parameter than non-linear approach [Dubey et al., 2016].

Table 5.9 Pseudo-first order and pseudo-second order kinetic parameters for linear analysis and non-linear analysis by customized Microcal origin

Analysis	**Customized**						
Kinetic model		**Pseudo-first order Parameter**			**Pseudo-second order Parameter**		
Temperature (K)	**q_e (exp.)**	**q_e (mg/g)**	**k_1 (1/min)**	**R^2 adj.**	**q_e (mg/g)**	**k_1 (1/min)**	**R^2 adj.**
303	0.47	0.351	0.39	0.18	0.55	0.44	0.692
313	0.44	0.342	0.37	0.16	0.50	0.42	0.659
323	0.41	0.432	0.34	0.14	0.47	0.39	0.719
333	0.38	0.512	0.33	0.11	0.39	0.38	0.745

for adsorption of chromium from aqueous solution on nano-alumina

5.2.4.3 Intra-particle diffusion

Later on, the process possibility was explored on the intra-particle diffusion model based on diffusive mass transfer where the adsorption rate expressed in terms of the square root of time (t). The following equation has been used [Weber and Morris, 1963]:

$$q_t = K_{id}\, t^{0.5} + C \qquad (5.11)$$

The plot of q_t vs. the square root of time at different temperatures has been shown in Figure 5.24 A. The values of intra-particle diffusion rate constant, K_{id} (mg $g^{-1}min^{-1/2}$) and

film thickness, C (mg g^{-1}) calculated from the intercept and slope of the plot, respectively along with their correlation coefficients has been presented in Table 5.10. Value of C gives an idea about the boundary layer thickness. Larger the value of C, greater will be the boundary layer effect on the adsorption process leading to a prominent role of surface adsorption in the rate-controlling step.

Table 5.10 Intra-particle diffusion constant values for removal of chromium from aqueous solution on nano-alumina

S. No.	Concentration (mg/L)	K_{id} (mg/g $min^{1/2}$)	C (mg/g)	R^2
1	5	0.32889	2.0497	0.98185
2	10	0.65274	3.3371	0.99147
3	15	1.06195	3.2197	0.95266
4	20	1.47935	2.6104	0.95552
5	25	1.79344	1.7191	0.94323

The intra-particle diffusion plot exhibited three linearity and has been demarcated into three regions as rapid external mass transfer (film diffusion) and intra-particle diffusion being represented as regions 1 and 2, respectively. The interior surface of adsorbent where adsorption occurred is represented by region 3. The probability of intra-particle

diffusion to be the rate-controlling step in the process has been ascertained by the plot that must pass through the origin (C=0) in diffusion controlled process, but in this case plots didn't pass through the origin. Further, the relatively high determination coefficient suggested intra-particle diffusion was not the only rate controlling in the process but might play a significant role in the beginning of the adsorption process [Mohanty et al., 2005; Stankovic´ et al., 2016].

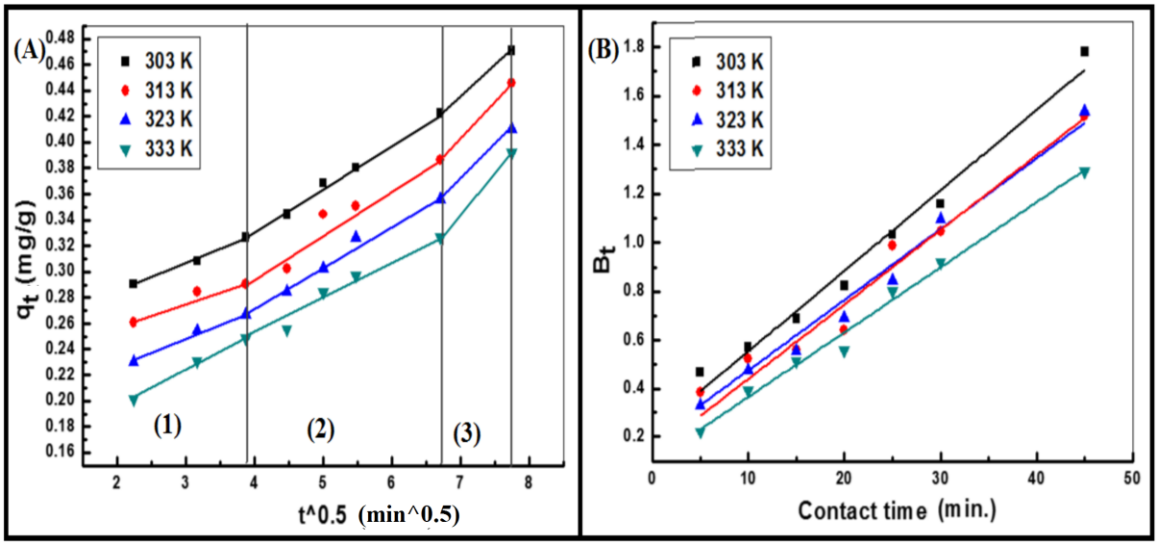

Figure 5.24 A) Intra-particle diffusion plot for removal of chromium from aqueous solution on nano-alumina. B) Boyd model plot for removal of chromium from aqueous solution on nano-alumina

5.2.4.4 Boyd model

In order to explore the probable mechanism of adsorption further, the Boyd model was applied on the kinetic data. This model distinguishes the film diffusion (boundary

layer) and pore diffusion (diffusion inside adsorbent pores). It can be expressed in the following form [Hu, et al., 2011]:

$$B_t = -0.4977 - ln\ (1 - F) \quad (5.12)$$

where, F is the fraction of adsorbed adsorbate at any time t (min). B_t was plotted against t and in the present case, the line (Figure 5.24 B) did not pass through origin. It indicated that adsorption has been governed by boundary layer diffusion mechanism.

5.2.5 Adsorption thermodynamic study

5.2.5.1 Effect of temperature

The influence of temperature on the removal of Cr (VI) has been investigated at different temperature ranges from 303 to 333 K and at various concentrations pre-defined for the experimentation. It was ascertained that percent removal slightly decreased with the temperature and this trend suggests the exothermic nature of the adsorption process as depicted in Figure 5.25. The probable reason behind this observation can be assigned to the enhancement of the relative escaping tendency of the adsorbate species from the solid phase to the bulk phase and a reduction in boundary layer thickness [Sharma and Weng 2007]. Consequently, lower temperature was found to be favorable for Cr(VI) removal from aqueous solutions.

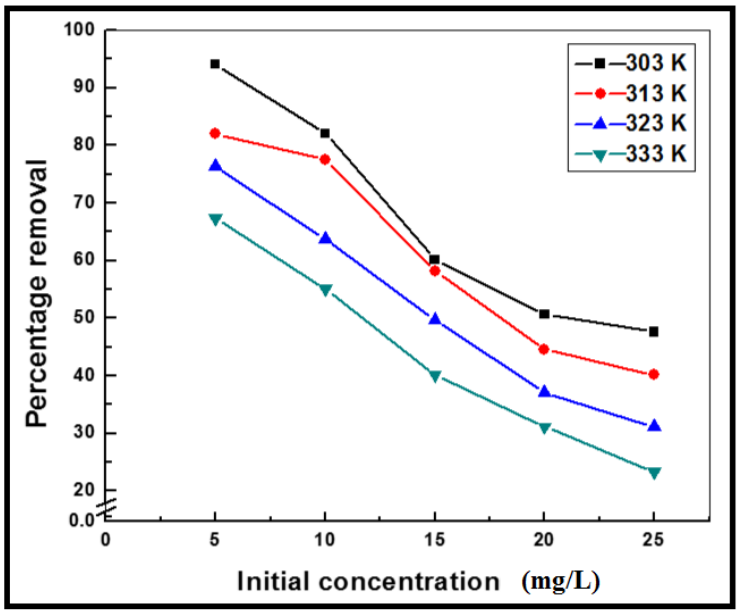

Figure 5.25 Effect of temperature on removal of Cr(VI) from aqueous solutions on nano-alumina

5.2.5.2 Thermodynamic parameters

Thermodynamic parameters such as changes in standard free energy (ΔG˚), enthalpy (ΔH˚), and entropy (ΔS˚) were evaluated from Langmuir adsorption model to confirm the adsorption nature of the present study. The following equations have been used for their estimation [Salvestrini et al., 2014; Brown et al., 2009; Elkady et al., 2011]:

$$\Delta G^{\circ} = - RT \ln K_L \quad (5.13)$$

$$\ln K_L = \Delta S^{\circ}/R - \Delta H^{\circ}/RT \quad (5.14)$$

where, ΔG° is the Gibbs free energy change, Langmuir constant b is considered as thermodynamic equilibrium constant; K_L (L mol^{-1}), R is universal gas constant (8.314

J•mol^{-1}•K^{-1}), and T is the absolute temperature in Kelvin. Subsequently, the values of ΔHº and ΔSº were also determined from the slope and intercept of the plot of ln K_L vs. 1/T, respectively. The values of ΔG°, ΔH° and ΔS° calculated at different temperatures have been tabulated in Table 5.11.

Table 5.11 Thermodynamic parameters for adsorption of chromium from aqueous solution on nano-alumina

S. No.	Temperature (K)	Δ G◦ (kJ mol^{-1})	ΔH◦ (kJ mol^{-1})	ΔS◦ (J mol^{-1} K^{-1})
1	303	-27.38	-75.81	-160.3
2	313	-26.47		
3	323	-24.10		
4	333	-21.27		

The negative ΔG◦ values affirm the feasibility of the adsorption process as well as the spontaneous nature of adsorption that do not require any external source of energy for its occurrence. Further, the decrement in negative value at higher temperature manifested that the spontaneity of adsorption process decline with rise in temperature. In case of physi-sorption, the change of standard free energy varies in the range of −20 to 0 kJ mol^{-1} while for involvement of chemi-sorption standard free energy varies in the range −80 and −400 kJ mol^{-1} [Avila et al. 2014)]. Furthermore, the (ΔH◦) values were also found to be

very low and negative (-75.81 kJ mol^{-1}) which indicated the physi-sorption of Cr(VI) on alumina nanoparticles which was also evident from various characterizations after adsorption besides exhibiting exothermic nature [Sharma et al. 2010]. The negative value -160.3 J mol^{-1} K^{-1} of entropy ($\Delta S\circ$) suggested that the adsorption process involves an associative mechanism as well as it reflected that no significant change occurred in the internal structures of the adsorbent during the adsorption process [Saha and Chowdhury 2011].

5.2.5.3 Activation energy

Activation energy is defined as the energy that must be overcome in order for a chemical reaction to occur. Being specific to adsorption processes, it is defined as the minimum energy needed for a specific adsorbate-adsorbent interaction to take place. The activation energy (E_a) for the adsorption of an adsorbate ion/molecule onto an adsorbent surface in an adsorption process can be evaluated from the Arrhenius equation as follows [Aksu, 2002]:

$$ln\ k_2 = ln\ A - E_a/RT \quad (5.15)$$

where, k_2 (g mg^{-1} min^{-1}) represents the rate constant obtained from the pseudo-second order kinetic model, E_a (J mol^{-1}) is the Arrhenius activation energy of adsorption and A is the Arrhenius factor. The values of E_a and A can be obtained from the slope and the intercept from the plot of ln k_2 versus 1/T (Figure 5.26). The activation energy was estimated as 4.2 kJ mol^{-1}. The magnitude of activation energy also suggests whether the

uptake of the adsorbate is governed by physical adsorption or by chemical adsorption. In the present case, low activation energy indicated the involvement of physical adsorption as the activation energy for physi-sorption is usually no more than 4.2 kJ mol^{-1} since the forces involved in physi-sorption are weak [Saha and Chowdhury 2011].

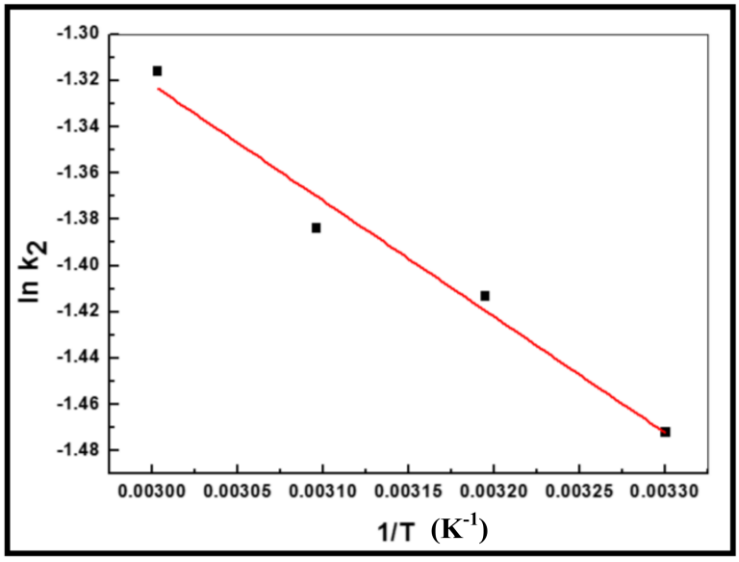

Figure 5.26 Arrhenius plot for removal of chromium from aqueous solution on nano-alumina

5.3 Desorption experiments

In order to corroborate the possibility of reuse of exhausted adsorbent desorption experiments were conducted with three desorbing agents namely NaOH (Sodium hydroxide), KOH (Potassium hydroxide) and NH_4OH (Ammonium hydroxide). 0.1N of the aforesaid solutions were used to desorb the adsorbed chromium ions from the

adsorbent and have shown desorption efficiencies of the order of 85.45 %, 84.82 % and 95.55 % respectively. Among all the solutions, maximum desorption efficiency has been exhibited by NH_4OH solution and thus it was selected for the desorption purpose. It was found that up to three cycles adsorbent exhibited considerable removal of chromium for reuse as an adsorbent after third cycle the desorption efficiency was reduced (Table 5.12).

Table 5.12 Chromium removal after subsequent regeneration cycle (Initial conc. =5mg/L, pH = 2.0, Dose = 10 g/L, Temperature =303 K)

S. No.	Regeneration cycle	Chromium removal (%)
1	1	97.95
2	2	96.45
3	3	92.37
4	4	79.93

5.4 Conclusions

RSM enables to estimate all linear and quadratic effects and 2-factor interactions, and requires less runs compared to conventional time-consuming experimental methods. The present study has demonstrated the application of three-factor-three-level box-behnken

design of RSM as an experimental tool for the first time to explain the effect of main operational parameters and their interactions for determining the conditions leading to high Cr (VI) uptake efficiency on alumina nanoparticles. An optimum condition for chromium uptake was achieved with RSM at initial chromium ion concentration of 5 mg/L, pH 2.03 and adsorbent dose of 10g/L for achieving 94% removal with desirability value of 1. Confirmatory experiments showed concordance of experimental values with that of the predicted values. According to the ANOVA results, the model presents high R^2 values of 96.51% for Cr(VI) ion removal efficiency, which indicates that the accuracy of the polynomial model was good. The time of equilibrium was 60 min. The isotherm data obtained for the system followed Langmuir model and kinetics was best elaborated by pseudo-second-order model. The negative value of Gibb's free energy change depicts the feasible and spontaneous nature of the process. The overall process of sequestration of Cr(VI) was exothermic in nature with positive value of entropy. The experimental results showed that under optimized conditions, nano-alumina can be used as an adsorbent for the removal of Cr(VI) from aqueous solutions.